Measurement of the frequency dependence of four terminal-pair air capacitors with a vector network analyzer

Stephan Schlamminger *Senior Member, IEEE*, Andrew Koffman *Senior Member, IEEE*, James Schmidt, Bryan Waltrip *Senior Member, IEEE*, and Yicheng Wang *Fellow, IEEE*

***Abstract*—Four terminal-pair air capacitors are important transfer standards to calibrate LCR meters up to a frequency of 10 MHz. We report a simple and new method to obtain the frequency dependence of the four terminal-pair capacitance of these standards using a four-channel vector network analyzer (VNA). The frequency dependence of the capacitance of an air capacitor and its uncertainty can be obtained from a single set of measurements without changing connections between the standard and the VNA, as has been the case in previously published work. The calculation of the frequency dependency is straightforward and model-independent. Nevertheless, an elementary model is provided to explain the observed frequency dependence. This article allows every laboratory with a four-channel VNA to measure the frequency dependence of these capacitors. Hence, a significant shortening of the traceability chain is achieved.**

***Index Terms*—Calibration, four terminal-pair, air capacitors, impedance measurement, frequency dependence**

I. Introduction

FOUR terminal-pair air capacitors are used in laboratories daily to calibrate and verify the operation of LCR meters, and, hence, these capacitors are an important standard in the toolbox of electrical metrology. Figure 1 shows a photograph of a typical set of four air capacitors with nominal values of 1 pF, 10 pF, 100 pF, and 1000 pF. The set shown in the photo was manufactured by Hewlett Packard[1]. Periodically, these capacitors are sent to a primary standard laboratory for calibration. There on each capacitor, two measurements are established: (1) the low-frequency (typically at 1 kHz) value of the three terminal-pair capacitance C_0, and (2) the frequency dependence $\varepsilon(f)$ of the capacitance relative to its low-frequency value, i.e., $C(f) = C_0(1 + \varepsilon(f))$. This article provides a simple method to measure $\varepsilon(f)$ with a commercially available four-channel network analyzer.

II. Literature review

In 1963, R.N. Jones published a technical note [1] describing a technique to extrapolate the measurements of capacitance at 1 kHz to higher frequencies. He assumed a series connection of a capacitor with a parasitic inductor and used a grid-dip meter to determine the resonant frequency of the combined circuit. For a 1000 pF capacitor, Jones found a serial inductance of 50 nH and determined a 9.7 % increase of the capacitance from low frequency to 10 MHz. The note by Jones was published before Cutkosky introduced the four-terminal pair impedance in a seminal article [2]. An updated version of the technical report was published considering the four-terminal definition [3] in 1980. Again, the measurement was performed with a grid-dip meter, but a more complicated circuit was adopted for the equivalent circuit of the capacitance standard.

Fig. 1. A commercial set of four standard air capacitors with nominal values of 1 pF, 10 pF, 100 pF, and 1000 pF.

A thorough theoretical analysis with simulation and measurements of the equivalent circuit components was performed and documented by Yonekura and Wakasugi. Both were working at the Yokogawa-Hewlett-Packard company in Japan [4] at the time.

At the same company, about a year later, the first systematic measurement without a grid-dip meter was carried out by Kiyoshi Suzuki [5]. He used a vector network analyzer to measure the reflection coefficient, S_{11}, as a function of frequency. Suzuki did not use the S parameter formalism. Instead, he used several measurements to obtain the four-terminal impedance of the standard. Two sets of measurements were performed at each port. In the first set, all other ports were left open, and in the second, one single port was shorted. The frequency dependence of the four-terminal pair impedance could be extrapolated to smaller frequencies from the eight data sets (four with open ports and four with one shorted). In many National Metrology Institutes (including the National Institute

[1]Certain commercial equipment, instruments, and materials are identified in this paper in order to specify the experimental procedure adequately. Such identification is not intended to imply recommendation or endorsement by the National Institute of Standards and Technology, nor is it intended to imply that the materials or equipment identified are necessarily the best available for the purpose.

of Standards and Technology), the Suzuki method became the de facto calibration method for these air capacitors [6], [7]. Suzuki published an improvement of his method specifically for large impedances [8] 2009. The improved method required an external shorting bar connected to the device.

In the meantime, researchers at NPL have developed a four-terminal pair bridge [9] capable of traceable measurements up to 1 MHz.

To our knowledge, Luca Callegaro and Francesca Durbiano at the National Metrology Institute in Italy applied for the first time the S parameter matrix to the problem [10], [11]. Researchers at the National Physical Laboratory in India use a similar method and provide a detailed report on their measurement [12]. Shorter reports from the National Institute of Metrology in Thailand can also be found in the literature on this topic [13], [14].

A collaboration between researchers from Italy and the UK explored a resonant method to estimate the change in capacitance [15]. Their method exploits one zero in the denominator of the expression for the four terminal-pair capacitance, $C_{4\mathrm{TP}}$. The model discussed in the present article uses every pole (zeros in the denominator) and zero in the numerator in our expression for $C_{4\mathrm{TP}}$.

Four channel vector network analyzers have been used recently in precision impedance measurements, for example, by researchers at the Swiss National Metrology Institute (METAS) to characterize calculable coaxial resistors [16].

III. Circuit Model and Theory

The simplest circuit model of the air capacitors is shown in Fig. 2. Its four terminal-pair impedance [2] is given by

$$Z_{4\mathrm{TP}} = Z_0\,(1 + Y_{hg}Z_h)\,(1 + Y_{lg}Z_l) + Z_h\,(1 + Y_{lg}Z_l) + Z_l\,(1 + Y_{hg}Z_h)\,, \quad (1)$$

as is derived in Appendix A. Except for the main impedance, $Z_0 = -i/(\omega C_0)$, all components shown Fig. 2 are parasitic.

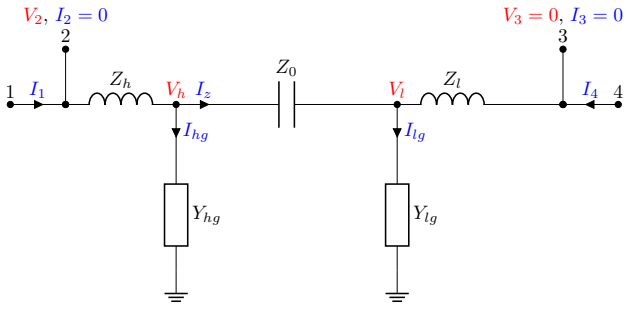

Fig. 2. The simplest model of a four terminal-pair air capacitor. Terminals one and four are the current terminals. The other two terminals are for the potential. The four terminal-pair definition of the impedance [2] requires the current to be zero at the potential terminals, $I_2 = I_3 = 0$, and the voltage to be zero at the low potential terminal, $V_3 = 0$.

To build intuition, we assume symmetric elements. The total serial impedance, an inductance, is abbreviated as $Z_s = i\omega L_s = Z_h + Z_l$ and the total admittance to ground, a capacitance as its sum $i\omega C_c/2 = Y_{hg} = Y_{lg}$. In practice, the capacitors are asymmetrical in construction; see Fig. 3. Nevertheless, the effect of the asymmetry on the conclusions reached in this article is negligible.

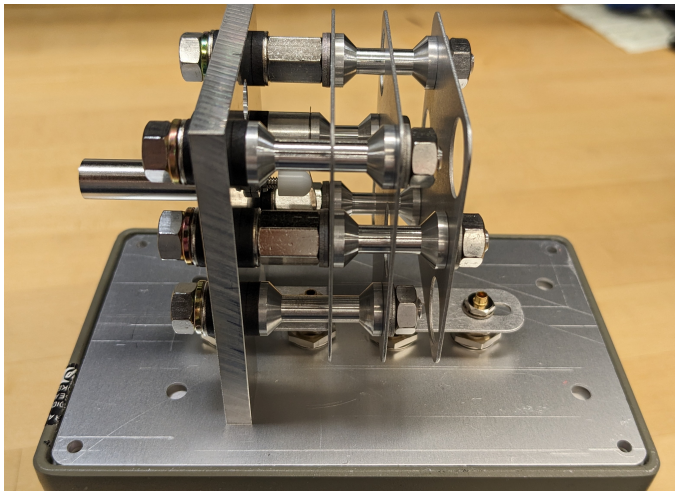

Fig. 3. The inside of the 10 pF capacitor. The asymmetry of the construction is visible. One capacitance electrode is the center plate, and the outer plates form the other. Because of the asymmetry, the leakage capacitance to the case must be different for the high and the low electrode, i.e., $Y_{hg} \neq Y_{lg}$.

Substituting the above expressions for the parasitic elements yields the four terminal-pair capacitance,

$$C_{4\mathrm{TP}}(f) \approx \frac{C_0 f_{p,1}^2}{f_{p,1}^2 - f^2}. \quad (2)$$

where the following definition was used

$$(2\pi f_{p,1})^2 = \frac{1}{C_+ L_s} \text{ with } C_+ = C_0 + C_c/4. \quad (3)$$

Eq. (2) is derived in Appendix B.

Expanding Eq. (2) in f to the second order obtains the relative change of the low-frequency capacitance. By rearranging the equation, the relative change in the capacitance, ε, from its low-frequency value can be introduced. It is

$$\varepsilon := \frac{C_{4\mathrm{TP}}(f)}{C_0} - 1 \approx \frac{f^2}{f_{p,1}^2}. \quad (4)$$

In Eq. 4, the Taylor expansion is truncated after the second order in f. This is a good approximation for $f \leq 30$ MHz. According to Eq. (4), the relative change of the capacitance is positive and proportional to f^2. The 1 pF air capacitor, however, defies this expectation, as the measured $C_{4\mathrm{TP}}$ decreases with rising frequency.

An explanation for the frequency dependency of the 1 pF air capacitor has been identified by Yonekura and Wakasugi [4]. For completeness, we reiterate their explanation: For low capacitance values, a common mode inductance plays a significant role, and the circuit diagram in Fig. 2 has to be modified to include that common inductor, as is shown in Fig. 4.

The admittances inside the dashed box in Fig. 4 can be reformulated using a Y-Δ transformation as is indicated in

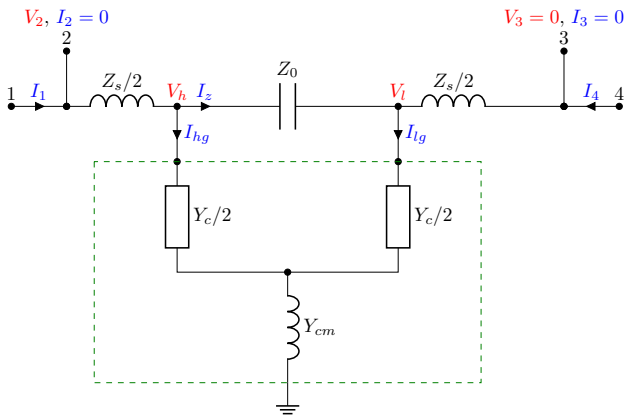

Fig. 4. Extended model with a common mode inductance in the leakage path.

Fig. 5. The admittances to the common point transform to a parallel but negative capacitance. According to the Y-Δ transformation and using $Y_c = i\omega C_c$ and $Y_{cm} = (i\omega L_{cm})^{-1}$, it is

$$Y_p = \frac{Y_c^2/4}{Y_c + Y_{cm}} = i\omega C_p \text{ and} \tag{5}$$

$$\frac{Y_g}{2} = \frac{Y_c Y_{cm}/2}{Y_c + Y_{cm}} = i\omega \frac{C_g}{2} \text{ with} \tag{6}$$

$$C_p = -\frac{C_c}{4}\frac{f^2}{f_{p,2}^2 - f^2}, \tag{7}$$

$$C_g = C_c \frac{f_{p,2}^2}{f_{p,2}^2 - f^2}, \text{ and } (2\pi f_{p,2})^2 = \frac{1}{C_c L_{cm}}. \tag{8}$$

Following Eq. (5) , a parallel capacitance with a negative value given by Eq. (7) must be added to the main capacitance C_0. With rising frequency, the parallel capacitance starts out small and grows more negative until it diverges at $f = f_{p,2}$. Above this frequency, C_p is positive. Also, according to Eq. 8, $C_g > C_c$. Hence, the experimental value of $f_{p,1}$ will be lower than calculated using $C_g \approx C_c$. This effect is particularly large for the 1 pF capacitor. In this case, the location of the first pole is a factor two lower than one would calculate by using the above approximation.

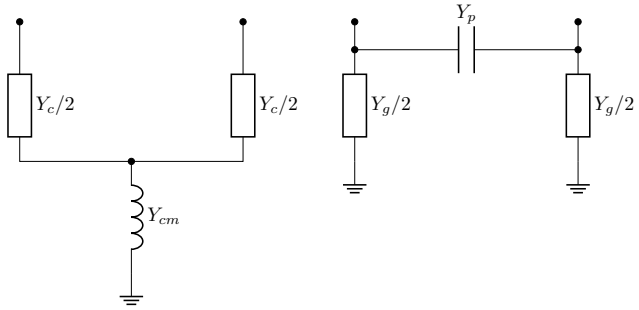

Fig. 5. Y-Δ transformation of the common mode admittance (an inductor) to a parallel (but negative) capacitance.

Adding the parasitic capacitance from Eq. (7) to C_0 in Eq. (2) yields

$$C_{4\mathrm{TP}}(f) = \frac{\left(C_0 - \frac{C_C}{4}\frac{f^2}{f_{p,2}^2 - f^2}\right) f_{p,1}^2}{f_{p,1}^2 - f^2}, \tag{9}$$

which can be rewritten to

$$C_{4\mathrm{TP}}(f) = -C_0 \frac{f_{p,1}^2 f_{p,2}^2}{f_{z,1}^2} \frac{f^2 - f_{z,1}^2}{(f^2 - f_{p,1}^2)(f^2 - f_{p,2}^2)} \text{ with} \tag{10}$$

$$f_{z,1}^2 = \frac{C_0}{C_+} f_{p,2}^2. \tag{11}$$

As indicated in Eq. 10, the four terminal-pair capacitance can be written as rational functions in f^2 with a single zero in the numerator at $f_{z,1}^2$ and two poles, $f_{p,1}^2$ and $f_{p,2}^2$ in the denominator. In this case, according to Eq. (11), the location of the zero is linked to the location of the second pole.

In general, allowing for n zeros and m poles, the functional form of $C_{4\mathrm{TP}}$ is

$$C_{4\mathrm{TP}}(f) = C_0\,(-1)^{n+m} \frac{f_{p,1}^2 \cdot f_{p,2}^2 \cdot \ldots \cdot f_{p,m}^2}{f_{z,1}^2 \cdot f_{z,2}^2 \cdot \ldots \cdot f_{z,n}^2} \frac{(f^2 - f_{z,1}^2)(f^2 - f_{z,2}^2) \cdot \ldots \cdot (f^2 - f_{z,n}^2)}{(f^2 - f_{p,1}^2)(f^2 - f_{p,2}^2) \cdot \ldots \cdot (f^2 - f_{p,m}^2)}, \tag{12}$$

where the prefactor in the first line ensures that $C_{4\mathrm{TP}} = C_0$ for $f = 0$. Taylor expanding Eq. (12) to fourth order yields,

$$\varepsilon = \frac{C_{4\mathrm{TP}}(f)}{C_0} - 1 = a_{zp} f^2 + b_{zp} f^4. \tag{13}$$

The index $_{zp}$ indicates that the coefficients a and b are obtained from the locations of the zeros and poles. They are

$$a_{zp} = \sum_i \frac{1}{f_{p,i}^2} - \sum_j \frac{1}{f_{z,j}^2} \text{ and} \tag{14}$$

$$b_{zp} = \sum_i \frac{1}{f_{p,i}^4} + \sum_{k>i} \frac{1}{f_{p,i}^2 f_{p,k}^2} - \sum_{i,j} \frac{1}{f_{p,i}^2 f_{z,j}^2} + \sum_{l>j} \frac{1}{f_{z,j}^2 f_{z,l}^2}, \tag{15}$$

where the indices obey

$$1 \le i \le m, \qquad i < k \le m, \tag{16}$$

$$1 \le j \le n, \quad \text{and} \quad j < l \le n. \tag{17}$$

A proof of the formulas for the coefficients for a_{zp} and b_{zp}, Eq. (14) and Eq. (15), respectively, is given in Appendix C.

IV. Measurements and Results

A four-channel vector network analyzer (VNA) (Rhode and Schwarz, Model ZNB8), together with the calibration device ZN-151 from the same manufacturer, is used to measure the scattering matrix of the standard. With the calibration device, automatic calibration of the VNA can be performed overnight. All calibrations and measurements shown below were taken in a frequency range from 10 MHz to 500 MHz. The capacitor under test is connected to the VNA via four RG-393 coax

cables with a length of 91 cm terminated by N male connectors on each end. On one side of each cable, an N(f)-to-BNC(m) adapter is necessary to connect to the capacitor, see Fig. 1. The connections are made as follows: channel 1 to high current port, channel 2 to high potential port, channel 3 to low potential port, and channel 4 to low current port.

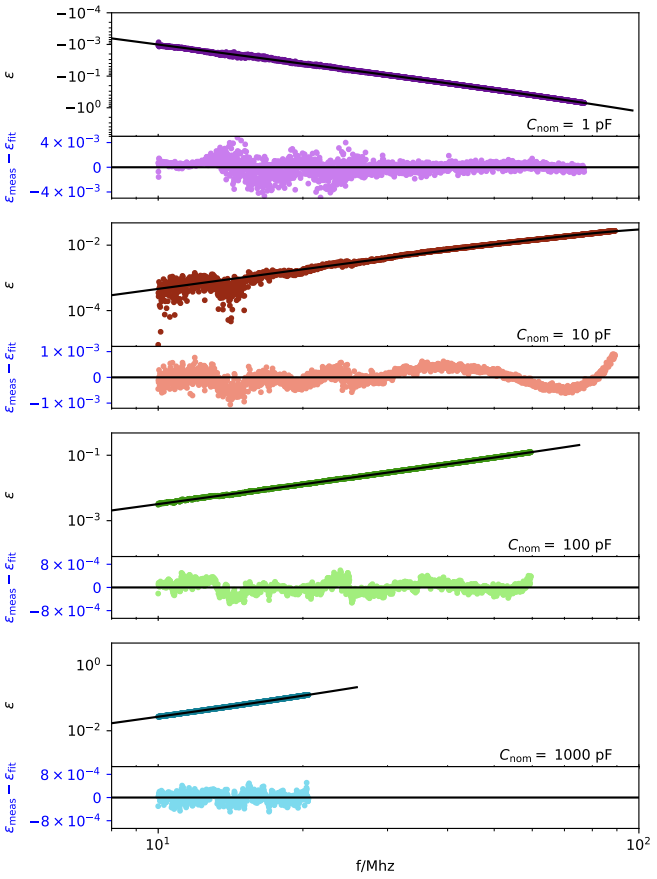

Fig. 6. The measured four terminal-pair capacitances as a function of frequency. Fits by the equation $\varepsilon = a_{\rm fit} f^2 + b_{\rm fit} f^4$ are shown as black lines. The fit residuals are plotted below each graph in lighter colors. The results of the fit $a_{\rm fit}$ and $b_{\rm fit}$ are shown in Table II and Table III, respectively. Only data in the frequency range $f_{\rm start} \le f \le f_{\rm end}$ are shown and considered for the fit. The values for $f_{\rm start}$ and $f_{\rm end}$ are given in Table I.

The four-by-four scattering matrix is

$$\mathbf{S} = (s_{jk}) \quad \text{with} \quad j,k \in \{1,2,3,4\}. \tag{18}$$

Conveniently, for a single capacitor, the complete $\mathbf{S}$ matrix at N discrete frequencies in the measurement interval can be measured by one setup. In previous work, two-channel VNAs were used, and the connection between the capacitor and the VNA had to be changed multiple times. With the four-channel VNA, measuring a single capacitance standard takes about 45 minutes. For the measurement, all channels are terminated with a characteristic impedance $Z_t = 50\,\Omega$. Then, the impedance matrix, as a function of frequency, can be obtained from the scattering matrix [17] using

$$\mathbf{Z} = Z_t \cdot (\mathbf{I} + \mathbf{S}) \times (\mathbf{I} - \mathbf{S})^{-1}, \tag{19}$$

where $\mathbf{I}$ denotes the 4×4 identity matrix and $(\mathbf{I} - \mathbf{S})^{-1}$ the matrix inverse of $\mathbf{I} - \mathbf{S}$. The impedance matrix links the four currents flowing through the four terminals (flowing into the standard with positive signs) to the four voltages, $\mathbf{V} = \mathbf{Z} \times \mathbf{I}$. Using the same numbering as in Fig. 2. We obtain the four terminal-pair impedance as

$$Z_{\rm 4TP} = \left.\frac{V_2}{-I_4}\right|_{V_3=0, I_2=0, I_3=0} = -z_{24} + \frac{z_{21} z_{34}}{z_{31}} \tag{20}$$

The measured four terminal-pair capacitance is then $C_{\rm 4TP,meas} = (-\mathrm{Im}(Z_{\rm 4TP})\,\omega)^{-1}$.

Plotting the change in capacitance as a function of frequency in a double logarithmic plot reveals, for low frequencies, a f^2 dependence, a line with slope two. To allow for a deviation from f^2 at higher frequency, we add a f^4 term. Hence, the simplest phenomenological function that can be fit to the data is

$$C_{\rm 4TP,fit} = C_0 \left(1 + a_{\rm fit} f^2 + b_{\rm fit} f^4\right) \tag{21}$$

The fit is performed such that

$$\chi^2 = \sum_1^N \left(C_{\rm 4TP,meas} - C_{\rm 4TP,fit}\right)^2 \tag{22}$$

is minimized. The parameters C_0, $a_{\rm fit}$ and $b_{\rm fit}$ are the result of the fit.

The fit function can be phenomenologically deduced from the measured data and is, hence, independent from the detailed model of the capacitor that has been discussed in Sec. III. The circuit model presented in Sec. III, and the analysis of the generalized capacitance function in f^2 with poles and zeros, lead to a functional form that is identical to the phenomenological form given by Eq. 21. Hence, we can compare the results of the phenomenological fit to the model-based prediction using the location of poles and zeros, see Sec. IV-B. Since Eq. 21 is model-independent, it can be applied to all four terminal-pair air and gas capacitors without detailed knowledge of their internal structure.

Figure 6 shows

$$\varepsilon := C_{\rm 4TP}/C_0 - 1, \tag{23}$$

for both, the measurement and the fit, for all four capacitors. The fit is carried out for frequencies ranging from $f_{\rm start} \le f \le f_{\rm end}$. We use $f_{\rm start} = 10\,\mathrm{MHz}$ and the end frequency is a third of the frequency of the first pole (defined below), i.e., $f_{\rm end} = \frac{1}{3}\min(f_{p1}, f_{p2})$. One-third was chosen because, at that frequency, the denominator differs from 1 by about 10 %, which is still reasonably small for a Taylor expansion. These and other statistics of the fit can be found in Table I. The last column of this table gives an estimate of the uncertainty of each measurement value obtained as

$$\langle \sigma_C \rangle = \sqrt{\frac{\chi^2}{N-3}}, \tag{24}$$

where $N - 3$ is the number of degrees of freedom of this fit.

The results and uncertainties of $a_{\rm fit}$ and $b_{\rm fit}$ are given in the first columns of Table II and Table III, respectively.

Besides the capacitance, the dissipation factor D can be obtained from the negative ratio of the real to the imaginary part of $Z_{\rm 4TP}$. The dissipation factors for the four capacitors

TABLE I
STATISTICS ON THE FIT. THE COLUMN LABELED $\langle\sigma\rangle$ GIVES THE ESTIMATED MEASUREMENT UNCERTAINTY OF EACH POINT BASED ON THE RESIDUAL SUM OF SQUARES; SEE TEXT FOR MORE INFORMATION.

nominal value C_{nom}/pF	start frequency f_{start}/MHz	end frequency f_{end}/MHz	number of points N	estim. unc. per point $\langle\sigma_C\rangle$/pF
1	10	77.0	2087	1.0×10^{-3}
10	10	89.3	2238	3.1×10^{-3}
100	10	59.7	1826	1.3×10^{-2}
1000	10	20.6	737	1.2×10^{-1}

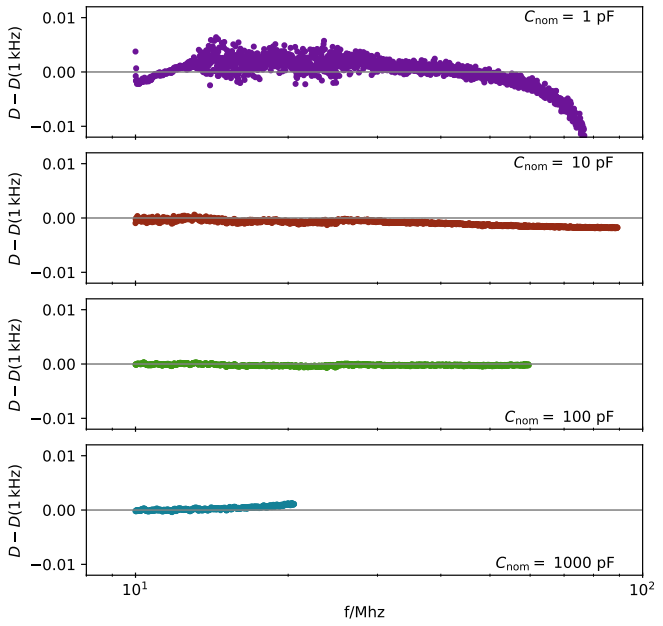

Fig. 7. The dissipation factor as a function of frequency obtained using $D = -\mathrm{Re}(Z_{4\mathrm{TP}})/\mathrm{Im}(Z_{4\mathrm{TP}})$. Fig. 9 shows D for a larger frequency range, including the poles. Here, the data is presented for the same frequency range as the data in Fig. 6.

as a function of frequency are given in Fig. 7. The data is shown for the same frequency range as in Fig. 6. The 10 pF and 100 pF data show a very weak dependence of D on f. Below 20 MHz, no significant dependence was found for both of these capacitors.

A. Uncertainty considerations

A full uncertainty analysis requires the discussion of Type A and Type B uncertainties. Here, we only present the discussion of the statistical uncertainties (Type A). A detailed investigation of the Type B uncertainties is ongoing and will be the topic of a future publication. Useful information on this topic can be found in [18] and [19]. Two strategies were used to obtain the Type A uncertainties of ε as a function of frequency: (1) conventional uncertainty propagation [20] and (2) bootstrap [21].

For conventional uncertainty propagation, σ_a^2 and σ_b^2 can be obtained from the product diagonal elements of the covariance matrix of the fit and $\langle\sigma_C^2\rangle$, given in Eq. (24). The uncertainty of ε is, then,

$$\sigma_\varepsilon(f) = \sqrt{\sigma_a^2 f^4 + \sigma_b^2 f^8 + 2r\sigma_a\sigma_b f^6}, \qquad (25)$$

where r is the correlation coefficient of a_{fit} and b_{fit}, which is in all four cases close to -1.

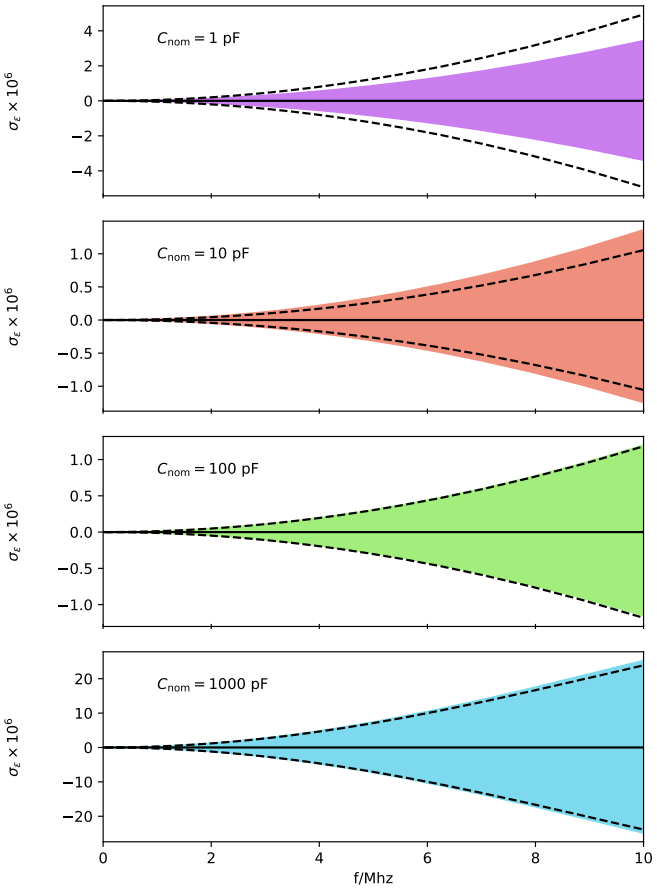

Fig. 8. The 1-σ uncertainty band of ε around its fit value (black solid lines) obtained with a bootstrap method (shaded) and classic uncertainty propagation (black dashed lines). The latter is a graph of $\pm\sigma_\varepsilon$ as given in Eq. (25).

One concern is that the choice of the start and end frequency of the fit biases the fit result. To assess such an effect, we used the bootstrap method. For each capacitance value, We artificially created 100 000 data sets from the existing data by choosing N data pairs with replacements from the N measurement pairs. From the obtained fits of the 100 000 data sets, ε was calculated for selected frequencies ranging from 0 to 10 MHz. For each frequency point, the band that contains 68.27 % of the data around $\varepsilon = a_{\mathrm{fit}} f^2 + b_{\mathrm{fit}} f^4$ was obtained.

Figure 8 shows the 1-σ uncertainty of ε obtained by both methods, uncertainty propagation and bootstrap. There is good agreement between both methods, and it is sufficient to provide the fit uncertainties. Furthermore, σ_ε is dominated by the term $\sigma_a f^2$, i.e., $\sigma_\varepsilon \approx \sigma_a f^2$, and this simplification is sufficient for all practical cases. Since no significant difference between the bootstrap method and the conventional error propagation was found, we conclude that the fit is mostly insensitive to the choice of the start and end frequency of the data.

TABLE II
RESULTS FOR THE PARAMETER a_{fit} FITTING EQ. (21) AND a_{zp} ACCORDING TO EQ. (14). THE NUMBER IN PARENTHESIS GIVES THE 1-σ UNCERTAINTIES OF THE APPROPRIATE DIGITS. THE LAST COLUMN SHOWS THE DIFFERENCE, $a_{zp} - a_{fit}$.

C_{nom} /pF	a_{fit} /MHz^{-2}	a_{zp} /MHz^{-2}	$(a_{\mathrm{zp}} - a_{\mathrm{fit}})$ /MHz^{-2}
1	$-1.0037(5) \times 10^{-4}$	$-1.00(4) \times 10^{-4}$	$0(4) \times 10^{-6}$
10	$4.62(1) \times 10^{-6}$	$6(4) \times 10^{-6}$	$1(4) \times 10^{-6}$
100	$3.208(1) \times 10^{-5}$	$3.2(4) \times 10^{-5}$	$0.4(40) \times 10^{-7}$
1000	$2.599(3) \times 10^{-4}$	$2.64(4) \times 10^{-4}$	$-0.4(40) \times 10^{-7}$

TABLE III
RESULTS FOR THE PARAMETER b_{fit} FITTING EQ. (21) AND b_{zp} ACCORDING TO EQ. (15). THE NUMBER IN PARENTHESIS GIVES THE 1-σ UNCERTAINTIES OF THE APPROPRIATE DIGITS. THE LAST COLUMN SHOWS THE DIFFERENCE, $b_{zp} - b_{fit}$.

C_{nom} /pF	b_{fit} /MHz^{-4}	b_{zp} /MHz^{-4}	$(b_{\mathrm{zp}} - b_{\mathrm{fit}})$ /MHz^{-4}
1	$-3.09(1) \times 10^{-9}$	$-2.63(2) \times 10^{-9}$	$4.58(14) \times 10^{-10}$
10	$-1.61(2) \times 10^{-10}$	$6.2(2) \times 10^{-12}$	$1.67(2) \times 10^{-10}$
100	$7.63(4) \times 10^{-10}$	$1.03(2) \times 10^{-9}$	$2.66(4) \times 10^{-10}$
1000	$8.88(6) \times 10^{-8}$	$6.910(2) \times 10^{-8}$	$-1.97(6) \times 10^{-8}$

B. More information on the zeros and poles

The section before obtains the frequency dependence of ε in a model-independent method. A simple function $af^2 + bf^4$, without concern of the physical model, was fitted to the measured values. Here, we make the connection of the fit to the theory of the capacitance.

According to Eq. (14) and Eq. (15), the coefficients a and b can also be obtained from the locations of the poles and zeros of $C_{4\mathrm{TP}}$ in the frequency domain.

The locations of zeros and poles of C_{4TP} can easily be found with the dissipation factor, $D = \mathrm{Re}(Y)/\mathrm{Im}(Y)$. With rising frequency D approaches $-\infty$ for zeros and $+\infty$ for poles of C_{4TP}, see Fig. 9. Searching for the poles in D and evaluating the functional dependence near the discontinuity allows one to detect and classify all poles and zeros in $C_{4\mathrm{TP}}$ for a given frequency range. In Fig. 9, the zeros are marked by circles and the poles by diamonds. The numerical values of the corresponding frequencies are listed in Table IV.

The a coefficient is obtained according to Eq. 14. The sign of a_{zp} is positive if $\sum f_{p,i}^{-2}$ is greater than $\sum f_{z,i}^{-2}$. That is the case for the three larger capacitors. Hence, only the 1 pF capacitor has a negative slope in Fig. 6, because of the low zero $f_{z,1}$. The calculated values of a_{zp} using Eq. 14 are given in Table II. The agreement with the corresponding parameter obtained from the fit is good and agree within uncertainties for all four standards. In the worst case, the difference is only $1.2 \times 10^{-6}\,\mathrm{MHz}^2$. This value was found for the 10 pF capacitor, which has the lowest frequency dependence of all four capacitors.

TABLE IV
ZEROS AND POLES AS OBTAINED FROM FIG. 9. BLANK SPACES INDICATE THAT THE FEATURE DOES NOT EXIST FOR $f \leq 500\,\mathrm{MHz}$.

C_{nom} /pF	$f_{z,1}$ /MHz	$f_{z,2}$ /MHz	$f_{p,1}$ /MHz	$f_{p,2}$ /MHz	$f_{p,3}$ /MHz
1	89.33		231.60	394.55	
10	240.19		268.04	329.05	
100	265.36		179.48	253.17	
1000	252.17	478.94	61.87	232.60	471.20

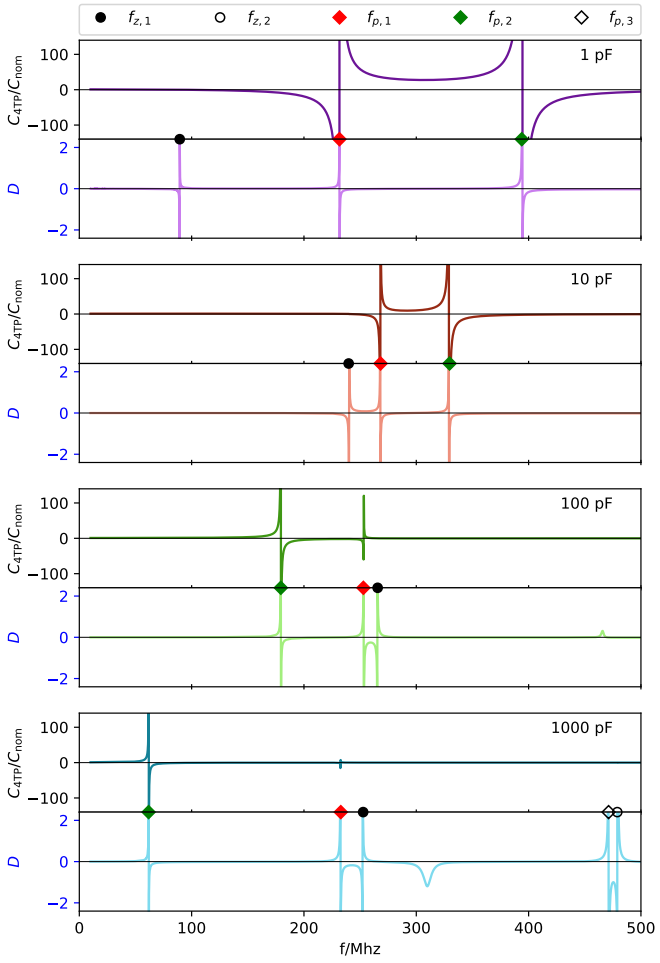

Fig. 9. Measurement of the capacitance divided by the nominal capacitance of all four capacitors as a function of frequency from 10 MHz to 500 MHz. The lower graphs, in a lighter color, show the dissipation factor D. It can be used to identify the zeros and poles in the measurement range.

The values for b_{zp} are given in Table III. The agreement between b_{zp} and b_{fit} is not quite as good, but at least they agree within an order of magnitude, except for the 1000 pF capacitor. Since the effect of the fit parameter b is very small for $f < 30\,\mathrm{MHz}$, this result is acceptable.

The physical model discussed in the theory section, Eq. (11) links the position of the $f_{z,1}$ and $f_{p,2}$ to the parasitic capacitance, according to

$$\frac{f_{p,2}^2}{f_{z,1}^2} - 1 = \frac{C_c}{4C_0} \tag{26}$$

TABLE V
COMPARISON OF THE PREVIOUS METHOD FOR CALIBRATION (TWO CHANNEL VNA) TO THE NEW METHOD (FOUR CHANNEL VNA). THE VALUES SHOWN IN THE TABLE ARE CALCULATED FOR $f_o = 10\,\mathrm{MHz}$. THE UNCERTAINTIES SHOWN IN THIS TABLE ARE EXPANDED WITH $k = 2$. FOR THE NEW METHOD ONLY TYPE A UNCERTAINTIES ARE GIVEN.

C_{nom} /pF	previous method $\varepsilon(f_o)$ $\times 10^3$	previous method $D(f_o)$ $\times 10^3$	new method $\varepsilon(f_o)$ $\times 10^3$	new method $D(f_o)$ $\times 10^3$
1	−13(14)	2(6)	−10.07(1)	−1.09(4)
10	1.4(11)	0.02(61)	0.461(2)	−0.218(4)
100	3.6(11)	0.07(11)	3.215(2)	−0.025(5)
1000	26.2(11)	1.4(14)	26.89(5)	1.04(3)

For the 1 pF and 10 pF capacitors, we calculate for C_c values of 74 pF and 34 pF, respectively. These values compare well to the ones given in [4], namely 66 pF and 54 pF, respectively. The fact that $f_{z,1} > f_{p,2}$ for the 100 pF and 1000 pF capacitors is hard to explain with the simple theory provided here. We suspect that there is a mechanism yet to be described that moves the first zero above f_{p2}.

Lastly, we note that in Table II $a_{zp} - a_{fit}$ is positive or very small for all cases. A possible explanation is that there is a zero above 500 MHz that is not considered. For example, if there were zero right at 500 MHz, a_{zp} would be lower by $4 \times 10^{-6}\,\mathrm{MHz}^{-2}$. Because of the possibility of an unknown pole and zero right outside the measurement area, the value $4 \times 10^{-6}\,\mathrm{MHz}^{-2}$ has been included as uncertainty for a_{zp} in Table II.

C. Comparison to previous results

Previously, at the National Institute of Standards and Technology (NIST), a two-channel vector network analyzer was used to measure ε and D as a function of frequency. Engineers working at the calibration service at NIST followed the Suzuki method [5], as described in [7]. The uncertainty analysis for the previous method is provided in [6].

Table V compares the results for ε and D calculated at a frequency of 10 MHz for the previous method and the new one described in this article. In all cases, the values agree within the combined uncertainties at $k = 2$.

Note that the uncertainties listed in Table V for the new method only include the Type A uncertainty. A complete uncertainty analysis is ongoing and will be the subject of a forthcoming publication. The excellent agreement between the two results implies that the Type B uncertainty of the method presented here is equal to or smaller than the uncertainty of the previous method. We note that the new method is less tedious and error-prone because the measurement can be performed in a single setup, and reconnecting the standard can be avoided.

V. CONCLUSION AND SUMMARY

This article shows a simple method to measure the frequency dependence of four terminal-pair air capacitors using a four-channel network analyzer. With a calibrated network analyzer, the measurement of one standard takes less than 45 minutes and can be made in one hook-up, i.e., no change in connection is required. The suggested measurement range is from 10 MHz to 500 MHz. We provide the equation to obtain the four terminal-pair capacitance from the four-by-four scattering matrix. The elements of the matrix, and hence, the four terminal-pair capacitances, are obtained for each frequency value.

The result is fitted to the function $\varepsilon = C_{4\mathrm{TP}}/C_0 - 1 = a_{fit} f^2 + b_{fit} f^4$. This function does not require a physical model and fits the measured data well. The data used for the fit ranges in frequency from 10 MHz to a third of the first resonance, i.e., 62 MHz for the 1000 pF, 180 MHz for the 100 pF and below 300 MHz for the other two capacitors.

Figure 10 summarizes the data and the fits previously shown in Fig. 6. The four terminal-pair capacitance decreases with increasing frequency for the 1 pF capacitor. For the other three nominal values, the capacitance increases. The absolute values of the slope of the fit line in a double logarithmic plot are all the same. The capacitance changes relatively by two decades for every decade in frequency, mostly due to the f^2 dependence of the data. For large frequencies, the beginning of the f^4 dependence can be seen for the 10 pF data.

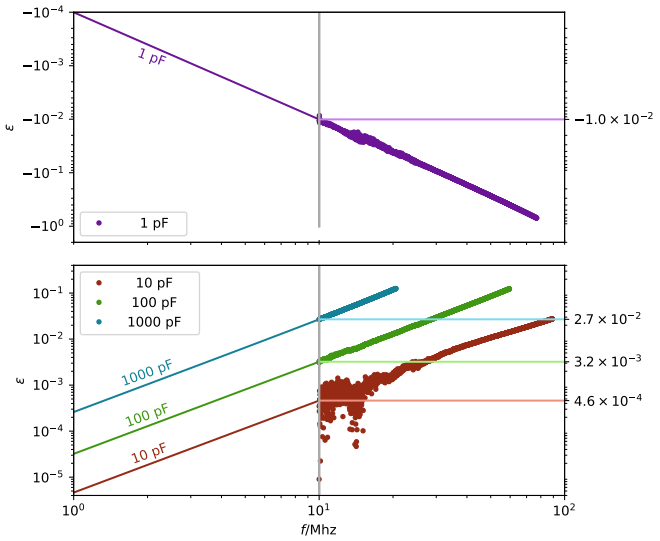

Fig. 10. Log-log plot of the value of $\varepsilon = C_{4\mathrm{TP}}/C_0 - 1$ as a function of frequency. For the 1 pF capacitor, the capacitance decreases, while for the other three, it increases with increasing frequency. The numbers on the right give the relative change of the capacitance value from low frequency to 10 MHz.

Finally, we provided a pedagocial model of the frequency dependence of the capacitance based on the location of the poles and zeros of $C_{4\mathrm{TP}}(f)$. We have shown that the physical model supports such an assumption. We have identified the zeros and poles for the four capacitances in a frequency range from 10 MHz to 500 MHz. With this model, the coefficients, a, could be predicted within their uncertainties. Remarkably, the model explains the negative frequency dependence of the 1 pF capacitor. Furthermore, this model explains the weak but positive frequency dependence of the 10 pF capacitor.

A noticeable feature in Fig. 10 is the relatively large scatter of the 10 pF data. This feature is, however, an artifact of

plotting the data on a logarithmic vertical scale. The ε values for the 10 pF are almost an order of magnitude smaller than the 100 pF values. Hence, the relative scatter is magnified by a factor of 10. As can be seen in Fig. 6, the residuals of ε about the fit function for the 10 pF are only slightly larger than those for the 100 pF capacitor.

Understanding the weak frequency dependence of the air capacitors at very low frequencies is an important stepping stone for impedance metrology at audio frequencies. At this frequency range, the air capacitors can be used as stable transfer standards, see, for example, [22].

APPENDIX A
DERIVATION OF THE FOUR TERMINAL-PAIR IMPEDANCE

Tracing the circuit diagram in Fig. 2 from right to left yields the following elementary relations:

$$\begin{aligned} V_l &= -I_4 Z_l, \\ I_{lg} &= V_l Y_{lg}, \\ I_z &= I_{lg} - I_4, \\ I_{hg} &= V_h Y_{hg}, \\ I_1 &= I_z + I_{hg}, \text{ and} \\ V_2 &= V_h + Z_h I_1. \end{aligned}$$

From a combination of these relationships, the four terminal-pair impedance is obtained as

$$\begin{aligned} Z_{4\mathrm{TP}} = \frac{V_2}{-I_4} \quad &= Z_0\left(1+Y_{hg}Z_h\right)\left(1+Y_{lg}Z_l\right) + \\ &Z_h\left(1+Y_{lg}Z_l\right) + Z_l\left(1+Y_{hg}Z_h\right) \end{aligned} \tag{27}$$

APPENDIX B
FROM THE FOUR TERMINAL-PAIR IMPEDANCE TO THE CAPACITANCE

Applying $Z_h = Z_l = i\omega L_s/2$ and $Y_{hg} = Y_{lg} = i\omega C_c/2$ to Eq. (27), yields

$$Z_{4\mathrm{TP}} = -i\frac{\left(\left(C_0+\frac{C_c}{4}\right)L_s\omega^2 - 1\right)\left(\frac{C_cL_s}{4}\omega^2 - 1\right)}{C_0\omega}. \tag{28}$$

The value of the four terminal-pair capacitance is given by $C_{4TP} = \left(-\mathrm{Im}(Z_{4TP})\omega\right)^{-1}$. Using the substitutions,

$$\begin{aligned} 2\pi f &= \omega, && (29)\\ C_+ &= C_0 + \frac{C_c}{4}, && (30)\\ (2\pi f_{p,1})^2 &= \frac{1}{L_sC_+}, \text{ and} && (31)\\ (2\pi f_{p,2})^2 &= \frac{1}{L_sC_c/4}, && (32) \end{aligned}$$

the capacitance evaluates to approximately,

$$\begin{aligned} C_{4\mathrm{TP}} &= \frac{C_0}{\left(f^2/f_{p,1}^2-1\right)\left(f^2/f_{p,2}^2-1\right)} \\ &= \frac{C_0 f_{p,1}^2 f_{p,2}^2}{\left(f^2-f_{p,1}^2\right)\left(f^2-f_{p,2}^2\right)}. \end{aligned} \tag{33}$$

The lower of the two poles, i.e., $f_{p,1}$, dominates the capacitance, and we can approximate,

$$C_{4\mathrm{TP}} \approx -\frac{C_0 f_{p,1}^2}{\left(f^2-f_{p,1}^2\right)}. \tag{34}$$

APPENDIX C
PROOF OF THE EQUATIONS FOR a_{zp} AND b_{zp}

Here, we prove that if the capacitance is given by a rational function in f^2 as

$$\begin{aligned} C_{n,m}(f) = C_0\left(-1\right)^{n+m}&\frac{f_{p,1}^2\cdot f_{p,2}^2\cdot\ldots\cdot f_{p,m}^2}{f_{z,1}^2\cdot f_{z,2}^2\cdot\ldots\cdot f_{z,n}^2} \\ &\frac{(f^2-f_{z,1}^2)(f^2-f_{z,2}^2)\cdot\ldots\cdot(f^2-f_{z,n}^2)}{(f^2-f_{p,1}^2)(f^2-f_{p,2}^2)\cdot\ldots\cdot(f^2-f_{p,m}^2)}, \end{aligned} \tag{35}$$

it can be Taylor expanded to the fourth order in f, resulting in

$$C_{(n,m)}(f) = C_0\left(1 + a_{n,m}f^2 + b_{n,m}f^4\right), \tag{36}$$

where the coefficients are given by

$$a_{n,m} = \sum_i \frac{1}{f_{p,i}^2} - \sum_j \frac{1}{f_{z,j}^2} \text{ and} \tag{37}$$

$$\begin{aligned} b_{n,m} = &\sum_i \frac{1}{f_{p,i}^4} + \sum_{k>i}\frac{1}{f_{p,i}^2 f_{p,k}^2} - \sum_{i,j}\frac{1}{f_{p,i}^2 f_{z,j}^2} \\ &+ \sum_{l>j}\frac{1}{f_{z,j}^2 f_{z,l}^2}, \end{aligned} \tag{38}$$

where the indices obey

$$1 \le i \le m, \qquad i < k \le m, \tag{39}$$

$$1 \le j \le n, \quad \text{and} \quad j < l \le n. \tag{40}$$

Different from the main text, we use here the index $_{n,m}$ to indicate the number of zeros and poles. This is required because we use complete induction to prove the above assertion. Note the trivial case,

$$C_{0,0} = C_0 \text{ hence } \; a_{0,0} = 0 \text{ and } \; b_{0,0} = 0, \tag{41}$$

For the cases $n = 1, m = 0$ and $n = 0, m = 1$, Eq. (37) and Eq. (37) simplify to

$$a_{1,0} = -\frac{1}{f_{z,1}^2}, \;\; b_{1,0} = 0, \tag{42}$$

and

$$a_{0,1} = \frac{1}{f_{p,1}^2} \text{ and } b_{0,1} = \frac{1}{f_{p,1}^4}. \tag{43}$$

The capacitance for one zero evaluates to

$$C_{1,0} = \frac{-C_0}{f_{z,1}^2}\left(f^2 - f_{z,1}^2\right) \approx C_0\left(1 - \frac{f^2}{f_{z,1}^2}\right) \tag{44}$$

and hence,

$$a_{1,0} = -\frac{1}{f_{z,1}^2} \text{ and } b_{1,0} = 0, \tag{45}$$

which is in agreement with Eq. (42). For the case $n = 0$ and $m = 1$, we perform a Taylor expansion to the fourth order and obtain,

$$C_{0,1}(f) = -C_0 f_{p,1}^2 \frac{1}{f^2 - f_{p,1}^2} \approx C_0 \left(1 + \frac{f^2}{f_{p,1}^2} + \frac{f^4}{f_{p,1}^4}\right). \tag{46}$$

Equation (46) translates to

$$a_{0,1} = \frac{1}{f_{p,1}^2} \text{ and } b_{0,1} = \frac{1}{f_{p,1}^4}, \tag{47}$$

which is identical to Eq. (43). With this, the beginning of the induction has been shown for both cases.

Adding an additional zero to $a_{n,m}$ leads, according to Eq. (37), to

$$a_{n+1,m} = a_{n,m} - \frac{1}{f_{z,n+1}^2} \text{ and} \tag{48}$$

$$b_{n+1,m} = b_{n,m} + \frac{1}{f_{z,n+1}^2} \left(\sum_{i=1}^{n} \frac{-1}{f_{p,i}^2} + \sum_{j=1}^{m} \frac{1}{f_{z,j}^2}\right). \tag{49}$$

Equation (49) can be succinctly expressed as

$$b_{n+1,m} = b_{n,m} - \frac{a_{n,m}}{f_{z,n+1}^2}. \tag{50}$$

Adding the additional zero to the capacitance equation leads to

$$C_{n+1,m} = C_{n,m} \frac{-1}{f_{z,n+1}^2} \left(f^2 - f_{z,n+1}^2\right). \tag{51}$$

Hence,

$$a_{n+1,m} = a_{n,m} - \frac{1}{f_{z,n+1}^2} \text{ and} \tag{52}$$

$$b_{n+1,m} = b_{n,m} - \frac{\alpha_{n,m}}{f_{z,n+1}^2} \tag{53}$$

Equations (52) and (53) agree with equations (48) and (56), respectively.

Adding an extra pole to Eq (37) and Eq (38) produces

$$a_{n,m+1} = a_{n,m} + \frac{1}{f_{p,m+1}^2} \text{ and} \tag{54}$$

$$b_{n,m+1} = b_{n,m} + \frac{1}{f_{p,m+1}^4} + \frac{1}{f_{p,m+1}^2} \left(\sum_{i=1}^{n} \frac{1}{f_{p,i}^2} - \sum_{j=1}^{m} \frac{1}{f_{z,j}^2}\right). \tag{55}$$

The second equation can be written as

$$b_{n,m+1} = b_{n,m+1} + \frac{1}{f_{p,m+1}^4} + \frac{a_{n,m}}{f_{p,m+1}^2}. \tag{56}$$

Adding the additional pole to the capacitance equation leads to

$$C_{n,m+1} = -C_{n,m} f_{p,m+1}^2 \frac{1}{f^2 - f_{p,m+1}^2} \tag{57}$$

Expanding up to f^4, multiplying out, and using $C_{n,m} = C_0(1 + a_{n,m} f^2 + b_{n,m} f^4)$, leads to

$$a_{n,m+1} = a_{n,m} + \frac{1}{f_{p,m+1}^2} \text{ and} \tag{58}$$

$$b_{n,m+1} = b_{n,m} + \frac{1}{f_{p,m+1}^4} + \frac{a_{n,m}}{f_{p,m+1}^2}. \tag{59}$$

Equation (58) is identical to Eq. (54), and so is Eq. (59) to Eq. (55). This concludes the proof.

REFERENCES

[1] R. N. Jones, A technique for extrapolating the 1 kc values of secondary capacitance standards to higher frequencies *National Bureau of Standards Technical Note* 201 (1963).

[2] R. D. Cutkosky, Four-terminal-pair networks as precision admittance and impedance standards. *IEEE Transactions on Communication and Electronics*, **83** (70), 19-22 (1964).

[3] R. N. Jones, Evaluation of three-terminal and four-terminal pair capacitors at high frequencies. *National Bureau of Standards Technical Note* 1024 (1980).

[4] T. Yonekura and T. Wakasugi. Frequency characteristics of four terminal pair air-dielectric capacitors. *Proc. Nat. Conf. Standards Laboratories (NCSL) Workshop and Symp.* (1990).

[5] K. Suzuki, Evaluation of three-terminal and four-terminal pair capacitors at high frequencies. *IEEE Transactions on Instrumentation and Measurement* **40**, 420-422 (1991).

[6] A. D. Koffman *et al.*, Uncertainty analysis for four terminal-pair capacitance and dissipation factor characterization at 1 and 10 MHz. *IEEE Transactions on Instrumentation and Measurement* **49** 346-348, (2000).

[7] S. Avramov-Zamurovic *et al.*, Evaluation of three-terminal and four-terminal pair capacitors at high frequencies. *IEEE Transactions on Instrumentation and Measurement* **49**, 398-404 (2000).

[8] K. Suzuki, A New Short-Bar Method for 4TP Admittance Standards Calibration by Using a Modified Z-Matrix Expression to Improve Signal-to-Noise Ratio (S/N) for Higher Impedances. *IEEE Transactions on Instrumentation and Measurement* **58**, pp. 980-984 (2009).

[9] S. A. Awan *et al.*, A new four terminal-pair bridge for traceable impedance measurements at frequencies up to 1 MHz *IEEE Transactions on Instrumentation and Measurement* **50**, 282-285 (2001).

[10] L. Callegaro and F. Durbiano, Four-terminal-pair impedances and scattering parameters. *Measurement Science and Technology* **14**, 523-529 (2003).

[11] L. Callegaro, The metrology of electrical impedance at high frequency: a review. *Measurement Science and Technology* **20**, 1-14 (2009).

[12] S. Singh *et al.*, Realization of Four-Terminal-Pair Capacitors as Reference Standards of Impedance at High Frequency Using Impedance-Matrix Method, *IEEE Transactions on Instrumentation and Measurement* **66** 2129-2135 (2017).

[13] P. Moonmirat, M. Homklintian and C. Kumtawee, "Measurement of the frequency dependence of standard capacitors in the frequency range 10 kHz to 1 MHz," *Conference on Precision Electromagnetic Measurements (CPEM 2016)*, Ottawa, ON, Canada, pp. 1-2(2016).

[14] M. Homklintian, Establishment of 4TP air-dielectric capacitance standard for 1 pF, 10 pF, 100 pF and 1000 pF in the frequency range up to 30 MHz at NIMT, *Conference on Precision Electromagnetic Measurements (CPEM 2020)*, Denver, CO, USA, pp. 1-2 (2020).

[15] S. A Awan, L. Callegaro and B. P Kibble, Resonance frequency of four terminal- pair air-dielectric capacitance standards and closing the metrological impedance triangle. *Measurement Science and Technology* **15**, 969-972 (2004).

[16] M. Agustoni, S. De Préville and F. Overney, "Broadband Calculable Coaxial Resistors," *IEEE Transactions on Instrumentation and Measurement*, **72** 1-10, (2023).

[17] D.M. Pozar, Microwave Engineering, 4th Ed. J. Wiley & Sons, 2012.

[18] M. Zeier, D. Allal, R. Judaschke, Guidelines on the Evaluation of Vector Network Analysers (VNA), *EURAMET Calibration Guide No. 12* Version 3, 3/2018 https://www.euramet.org/Media/news/I-CAL-GUI-012_Calibration_Guide_No._12.web.pdf.

[19] L. Callegaro, M. Sellone and N. Shoaib, "On the uncertainty of network analysis methods for the calibration of electrical impedance standards at high frequency," 2017 *IEEE International Instrumentation and Measurement Technology Conference* (I2MTC), Turin, Italy, pp. 1-5 (2017).

[20] B. N. Taylor and C. E. Kuyatt, Guidelines for Evaluating and Expressing the Uncertainty of NIST Measurement Results *NIST Technical Note 1297* 1297 (1994).
[21] B. Efron Bootstrap Methods: Another Look at the Jackknife, P*Ann. Statist.* **7** (1979).
[22] M. Feige *et al.*, Comparison of a 100-pF Capacitor With a 12906-Ω Resistor Using a Digital Impedance Bridge *IEEE Transactions on Instrumentation and Measurement* **71** 1 (2022).

Stephan Schlamminger (Senior Member, IEEE) received the Diploma degree in physics from the University of Regensburg, Regensburg, Germany, in 1998, and the Ph.D. degree in experimental physics from the University of Zurich, Zürich, Switzerland, in 2002. His thesis was on the determination of the Newtonian constant of gravitation, G. From 2002 to 2010, he has worked with the University of Washington, Seattle, WA, USA, on an experimental test of the equivalence principle. In 2010, he moved to the National Institute of Standards and Technology (NIST), Gaithersburg, MD, USA, and began working on the Kibble balance. In 2016, he became the Leader of the Fundamental Electrical Measurement (FEM) Group. From 2017 to 2018, he was with the Regensburg University of Applied Science, Regensburg, where he taught physics. He moved back to NIST in 2018 and is a Physicist with the FEM Group.

Andrew D. Koffman (Senior Member, IEEE) received the B.S. degree from the University of Maryland at College Park, College Park, MD, USA, in 1988, and the M.S. degree from Vanderbilt University, Nashville, TN, USA, in 1990, all in electrical engineering. He joined the Electricity Division (now Quantum Measurement Division), National Institute of Standards and Technology, Gaithersburg, MD, USA, in 1990. He has worked to develop and apply model-based strategies for testing complex electronic systems and currently works in the area of ac impedance metrology.

James W. Schmidt received a B.A. in physics from the University of Wyoming at Laramie, Wyoming, U.S.A (1970). While there he built and calibrated altimeters for balloon flights used for investigating gamma radiation at high altitudes. Drafted into the U.S. Army (1971-1973) he set to work operating unique research equipment at a lab in Maryland. He received an M.S. (1976) for measuring the libron-vibration modes in solid CO2 at high pressure, 8 kbar, and a Ph.D (1980) from the University of Delaware at Newark, Delaware, U.S.A. Data for the thesis was collected at the research reactor at Risø, Roskilde Denmark; publication title "Coherent Inelastic Neutron Scattering Study of Solid Ortho-deuterium at High Pressure", Phys. Rev. B. Vol 30, 6308 (1984). Since receiving his Ph.D he has worked at NBS in Gaithersburg, Maryland, U.S.A., later renamed NIST, and is now retired.

While at NIST he has worked on: Wetting Phenomena; Interfacial tension at vapor/liquid interfaces, and solid/liquid interfaces (1980-1990); on Refrigerant Properties (1990-2000); on Pressure Calibration Services (1999-2003); on Atomic Pressure Standards based on the polarizability of helium (2003-2010); on Novel Uses for acoustic and microwave resonances (2011-2015); on Micro-Fluidics calibrations (2015-2017).

Since retiring from NIST he has collaborated with colleagues at INRIM, Torino Italy; at the BIPM, in Sevres, France; and at CNAM in Saint Denis, Paris, France.

Bryan C. Waltrip (Senior Member, IEEE) was born in Chicago, IL, USA. He received the B.S. degree in electrical engineering and computer science from the University of Colorado, Boulder, CO, USA, in 1987, and the M.S. degree in electrical engineering from Johns Hopkins University, Baltimore, MD, USA, in 1998. Since 1987, he has been an Electronics Engineer with the Quantum Measurement Division, National Institute of Standards and Technology, Gaithersburg, MD, USA, where he is currently involved in the development of high-accuracy measurement systems in the areas of ac voltage, current, power, ratio, phase, and impedance.

Yicheng Wang (Fellow, IEEE) received the Ph.D. degree in atomic physics from the College of William and Mary, Williamsburg, VA, USA, in 1987. He was a Post-Doctoral Associate with the College of William and Mary until 1989. From 1990 to 1996, he was a Research Staff with the Notre Dame Radiation Laboratory, U.S. Department of Energy, Notre Dame, IN, USA. In 1996, he joined the National Institute of Standards and Technology, Gaithersburg, MD, USA, where he has been with the Quantum Measurement Division and currently the Leader of the Farad and Impedance Metrology Project. His current research interests include precision ac measurements and impedance standards.